Au nanorods-incorporated plasmonic-enhanced inverted organic solar cells*

Peng Ling(彭 玲)[a)b)§], Mei Yang(梅 杨)[a)§], Chen Shu-Fen(陈淑芬)[a)†], Zhang Yu-Pei(张玉佩)[a)], Hao Jing-Yu(郝敬昱)[a)], Deng Ling-Ling(邓玲玲)[a)b)], and Huang Wei(黄 维)[a)c)‡]

[a)] *Key Laboratory for Organic Electronics and Information Displays & Institute of Advanced Materials, Nanjing University of Posts & Telecommunications Synergistic Innovation Center for Advanced Materials, Nanjing* 210023, *China*

[b)] *School of Opto-Electronic Engineering, Nanjing University of Posts & Telecommunications, Nanjing* 210023, *China*

[c)] *Key Laboratory of Flexible Electronics & Institute of Advanced Materials, National Synergistic Innovation Center for Advanced Materials, Nanjing Tech University, Nanjing* 211816, *China*

(Received 3 April 2015; revised manuscript received 1 June 2015; published online 12 October 2015)

The effect of Au nanorods (NRs) on optical-to-electric conversion efficiency is investigated in inverted polymer solar cells, in which Au NRs are sandwiched between two layers of ZnO. Accompanied by the optimization of thickness of ZnO covered on Au NRs, a high-power conversion efficiency of 3.60% and an enhanced short-circuit current density (J_{SC}) of 10.87 mA/cm^2 are achieved in the poly(3-hexylthiophene): [6,6]-phenyl-C61-butyric acid methyl ester (P3HT:PC$_{60}$BM)-based inverted cell and the power conversion efficiency (PCE) is enhanced by 19.6% compared with the control device. The detailed analyses of the light absorption characteristics, the simulated scattering induced by Au NRs, and the electromagnetic field around Au NRs show that the absorption improvement in the photoactive layer due to the light scattering from the longitudinal axis and the near-field increase around Au NRs induced by localized surface plasmon resonance plays a key role in enhancing the performances.

Keywords: organic solar cells, nanorods, LSPR effect, scattering

PACS: 52.35.Hr, 52.25.Tx, 68.37.Lp, 68.37.Ps **DOI:** 10.1088/1674-1056/24/11/115202

1. Introduction

Polymer-fullerene bulk heterojunction solar cells (SCs) composed of interpenetrating networks of electron donors and acceptors, are now attracting a great deal of attention and show increasing importance due to their flexibility, low-cost, and simple manufacture process. However, a low charge mobility and a high bandgap for most of polymers lead to the carrier recombination and the limitation of the light absorption in an infrared region, thus restricting the overall performances of these polymer SCs (PSCs).[1,2] The recent developments of narrow-bandgap photoactive materials and employing tandem structures are efficient to broaden the light absorption band of the active layer, thus enhancing the power conversion efficiency (PCE) of PSCs to over 9%.[3–5] In addition, incorporating metallic nanoparticles (NPs) into devices to enhance light harvesting is also an attractive approach to improving the performances of SCs. Metallic NPs are well known for their strong interactions with electromagnetic waves due to the collective oscillations of the conduction electrons within the metallic particles.[6–8] This near-field strength generated by the localized surface plasmon resonance (LSPR) is beneficial to improving light harvesting in the photoactive layer,[9] and hence increasing the short-circuit current density (J_{SC}) and PCE in organic solar cells (OSCs).

The devices made via incorporating Au or Ag NPs into a carrier extraction layer,[10–12] a photoactive layer,[13–15] or depositing them onto the electrode surface,[16–18] have been widely reported with significant performance improvement. One of the most significant PCE enhancements was reported,[18] in which an enhancement factor of 70% was obtained through inserting Ag NPs below the poly(3,4-ethylenedioxythiophene): poly(4-styrenesulfonate) (PEDOT:PSS) layer. Unfortunately, its overall efficiency was rather low. Qu *et al.*[19] numerically simulated the absorption enhancement values using the finite element method with a three-dimensional model and demonstrated that plasmonic enhancement of above 100% could be obtained by optimizing the shapes, the sizes, and the positions of Ag NPs. However, despite these reports on performance improvement, a significant PCE degradation was also observed when Ag NPs without being capped by any insulator shell were embedded into a photoactive layer[20] and the continuous decline of PCE with the increase in Ag NPs concentration revealed that the intimate contact between the metallic NPs and the photoactive

*Project supported by the Ministry of Science and Technology, China (Grant No. 2012CB933301), the National Natural Science Foundation of China (Grant Nos. 61274065, 51173081, 61136003, BZ2010043, 51372119, and 51172110), and the Priority Academic Program Development of Jiangsu Provincial Higher Education Institutions and Synergetic Innovation Center for Organic Electronics and Information Displays, China.

§These authors contributed equally to this work.

†Corresponding author. E-mail: iamsfchen@njupt.edu.cn

‡Corresponding author. E-mail: iamdirector@fudan.edu.cn

© 2015 Chinese Physical Society and IOP Publishing Ltd

layer would promote trap-assisted recombination and degrade the performance of the plasmonic SCs. On the other hand, simulation results in the literature indicated that the near-field intensity induced by LSPR is commonly confined in a range of $\sim$ 20 nm around metallic NPs surface, and at the position far away from NPs surface, the local field weakens very quickly,[21–23] resulting in no improvement in absorption of the photoactive layer. Hence, the distance between NPs and photoactive layer must be considered to obtain an obvious performance enhancement.

The LSPR wavelength is another important factor influencing the optimization of performances in plasmonic PSCs. Several reports have demonstrated that the greater enhancement in PCE was observed when the extinction peak wavelength of metallic NPs was located in a poor light absorption region instead of near the absorption peak of the photoactive material.[24,25] At this point, the improvement on photocurrent using spherical Ag or Au NPs is restricted because of their LSPR peaks around 430 nm and 530 nm, respectively. Compared with nanospheres (NSs), rod-shaped metallic NPs exhibit a very good performance due to their widely tunable resonance peaks from the visible to near-infrared region by a simple alteration of longitudinal/transverse ratio. Janković *et al.*[24] reported a 14.4% PCE increase by inserting Au/SiO_2 core/shell nanorods (NRs) with an extinction peak of 830 nm into poly [2,6-4,8-di (5-ethylhexylthienyl) benzo [1,2-b; 3,4-b] dithiophene-alt-5-dibutyloctyl-3,6-bis (5-bromothiophen-2-yl) pyrrolo [3,4-c] pyrrole-1,4-dione]: [6,6]-phenyl-C_{61}-butyric acid methyl ester (PBDTT-DPP:PC_{60}BM), which is far higher than the PCE value of the same structure Au/SiO_2 core/shell NSs. In Lu *et al.*'s research,[25] employing Au NRs with transverse and longitudinal axes of 15 nm and 40–50 nm into PEDOT:PSS also shows good behaviors including photocurrent and PCE compared with those with Au NSs.

In this paper, we report a plasmonic-enhanced PSC based on Au NRs and instead of the commonly used PEDOT:PSS, ZnO is used as the ambient medium around Au NRs due to its significantly high refractive index, which will generate an obviously enhanced near-field intensity around Au NRs. Considering a quick electric field attenuation with distance, the ZnO thickness between the photoactive layer and Au NRs is vital and explored in this paper in order to obtain an improved device performance. Results demonstrate that 28-nm ZnO as the electron extraction layer generates the highest cell performance and has an optimized Au NRs' distribution density and distance to the active layer, a 19.6% PCE enhancement is observed compared with those without Au NRs. The possible influence factors including changes in the light field inside the device and scattering induced by Au NRs are investigated to explore the origin of performance improvement.

2. Experiment

The solution of the photoactive layer was prepared as follows. The mixed solution consisting of poly(3-hexylthiophene) (P3HT) and PC_{60}BM were dissolved into 1,2-dichlorobenzene with a concentration of 15:15 mg/mL and stirred at 50 °C overnight in a N_2-filled glove box. The ZnO precursor was prepared by dissolving zinc acetate dihydrate and monoethanolamine in ethanol solution, respectively, with concentrations of 21.9 mg/ml and 6.7 μL/ml, followed by at least 12 hours of stirring at 60 °C.

Figure 1(a) shows the absorption spectrum of Au NRs in aqueous solution and the inset shows the transmission electron microscopy (TEM) image of Au NRs. Their average lengths of longitudinal and transverse axes are 42 nm and 12 nm, corresponding to the LSPR peaks of 515 nm and 713 nm, respectively. The statistics on the aspect ratio (AR) of Au NRs in Fig. 1(b) shows that the ARs for most Au NRs used in our experiment fall in a range of 2.9–3.5. The Au NRs were obtained by centrifuging twice at 14000 rpm for 10 min to remove dispersant, and then dispersed in deionized water again by vigorously stirring to prevent their aggregation. Note that prior to spin coating, the solution containing Au NRs should be sonicated for at least 20 min to ensure that the Au NRs are well dispersed.

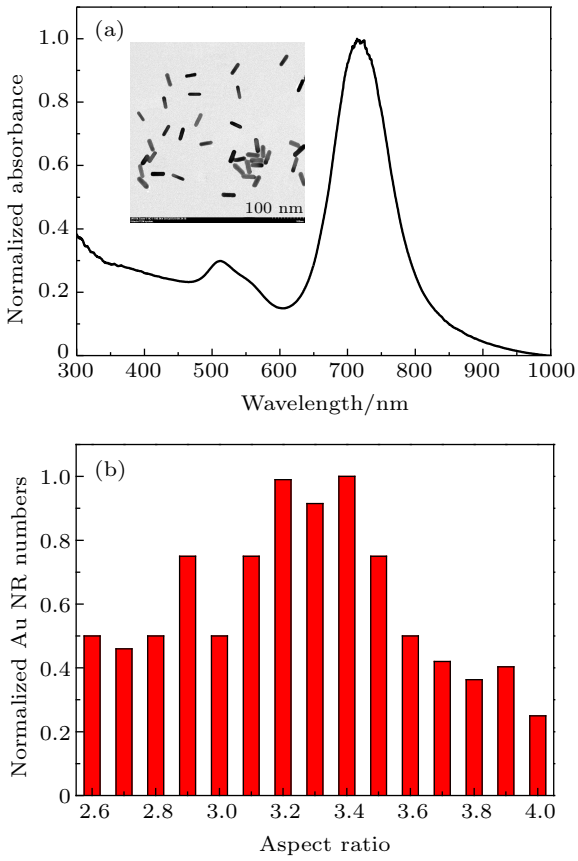


Fig. 1. (color online) (a) UV–vis absorption spectrum of Au NRs in aqueous solution. The inset shows the TEM image of Au NRs with a bar of 100 nm in length. (b) Statistics on the Au NRs' ratios from 400 particles in the TEM image.

Inverted devices were fabricated on patterned ITO-coated glass substrates. The substrates were washed by sonication in acetone, ethanol, and deionized water for 10 min, in sequence, and then dried at 100 °C for 10 min in an ambient atmosphere. Before spin-coating Au NRs, a 20-nm ZnO film was formed onto the cleaned ITO-coated substrate by spin-coating ZnO precursor at 3000 rpm for 60 s and subsequently pyrolysis on a hot plate in air at 150 °C for 30 min. The solution containing Au NRs was then spin-coated onto the ZnO layer, followed by 5 min drying at 100 °C to evaporate the solvent. After that another ZnO overlayer ranging from 4 to 20 nm was deposited, followed by pyrolyzation at 150 °C for 20 min. The thickness of the ZnO overlayer is controlled by adjusting the spin-coating speed and measured with ellipsometry. The ZnO-covered substrates were transferred into the glove box, followed by spin-coating the P3HT:$PC_{60}BM$ blend layer at 800 rpm for 60 s with an approximate film thickness of 70 nm. The film was then solvent annealed for 90 min in the glove box at room temperature. Finally, the devices were completed by sequential thermal evaporation of an 8-nm MoO_3 hole extraction layer and an 80-nm Ag anode under a high vacuum of 6.0×10^{-4} Pa. The device structure is shown in Fig. 2.

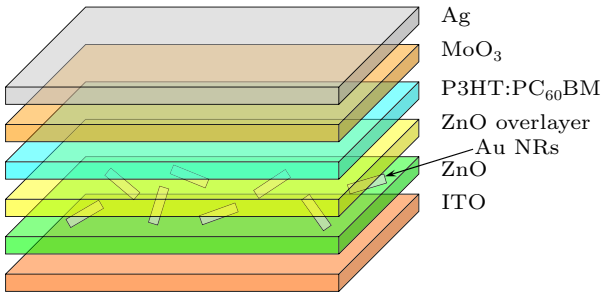


Fig. 2. (color online) Schematic structure for our cells.

Photovoltaic characteristics were measured with a solar simulator (Oriel 94023A, AAA, 300 W, USA) with an AM 1.5 G filter (Oriel, USA). The power of the simulated light was calibrated to 100 mW/cm^2 by using an Oriel Solar standard Si solar cell. The curves of current density versus voltage (J–V) were measured with a Keithley 2400 source meter and recorded with a computer. The absorption spectra were studied using ultraviolet (UV)–visible spectroscopy (Shimadzu UV-3600). Scanning electron microscope (SEM) imaging was carried out with JEOL JSM-6700 SEM system. The curves of incident photon versus conversion efficiency (IPCE) were measured with normal incident light from the monochromator (Oriel Instrument, model 74100).

3. Results and discussion

Three groups of devices are fabricated with different ZnO cathode buffer layer thickness values, where 20 nm ZnO/Au NRs/20 nm ZnO overlayer, 20 nm ZnO/Au NRs/8 nm ZnO overlayer, and 20 nm ZnO/Au NRs/4 nm ZnO overlayer are denoted as groups 1, 2, and 3. Note that in each group the control device that does not contain Au NRs but has the same ZnO thickness as that in the device with Au NRs, is also fabricated for comparison. Keeping the same ZnO thickness in each group would eliminate the difference in electron transport ability induced by the ZnO thickness variance. Figure 3(a) shows the J–V characteristic curves for all SCs under AM1.5 illumination. The results show that both the plasmonic device and the control device with an 8-nm ZnO overlayer exhibit the best performances in the three groups of devices. The Au NRs-incorporated device with an 8-nm ZnO overlayer exhibits a PCE enhancement factor of about 19.6% compared with that of its control device. The detailed parameters are listed in Table 1, and the increase in J_{SC} is mainly responsible for the performance improvement, which increases from 8.90 mA/cm^2 to 10.51 mA/cm^2 accompanied by the employment of Au NRs.

To analyze the origin of the increase in J_{SC}, we first measure the IPCE curves for the device with 20 nm ZnO/Au NRs/8 nm ZnO overlayer and its control device without Au NRs. As shown in Fig. 3(b), the device with incorporating Au NRs exhibits obviously increased IPCE values in a range

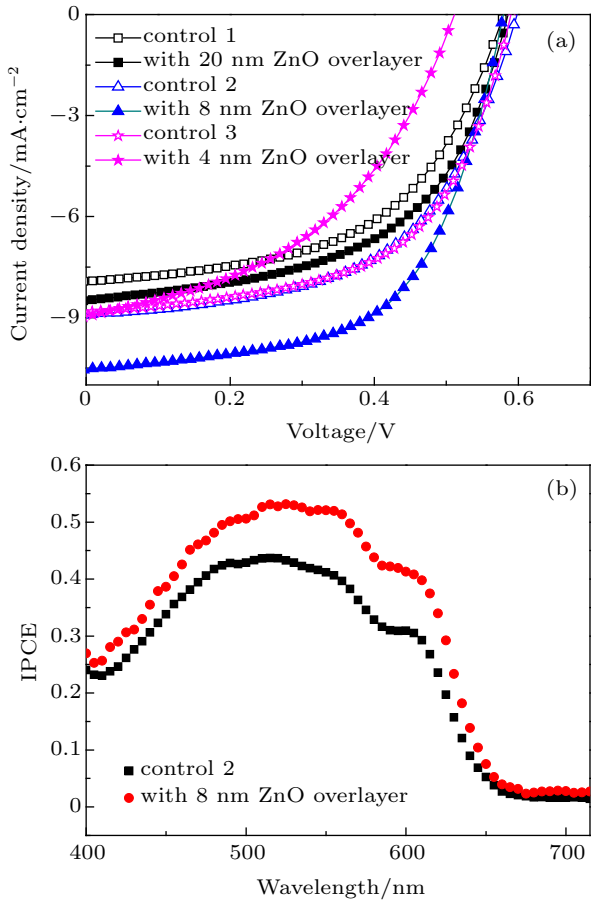


Fig. 3. (color online) (a) J–V characteristic curves for the plasmonic devices with various thickness values of ZnO overlayer and their control devices without Au NRs. (b) IPCE curves for the plasmonic device with an 8-nm ZnO overlayer and its control device.

Table 1. Photovoltaic characteristics for the plasmonic device with various thickness values of ZnO overlayer and its control device.

	Device	J_{SC}/mA·cm^{-2}	V_{OC}/V	FF	PCE/%
group 1	control 1	7.91	0.58	0.54	2.46
	with 20 nm ZnO overlayer	8.47	0.58	0.55	2.69
group 2	control 2	8.90	0.58	0.58	3.01
	with 8 nm ZnO overlayer	10.51	0.58	0.59	3.60
group 3	control 3	8.82	0.58	0.58	2.97
	with 4 nm ZnO overlayer	8.97	0.51	0.45	2.05

of 450–620 nm, with the peak value of efficiency enhanced from 0.43 to 0.53 at 525 nm. The theoretical J_{SC} value converted from the IPCE curve is 8.35 mA/cm^2 for the 8-nm ZnO overlayer device, showing a 20.3% enhancement factor compared with 6.94 mA/cm^2 in the control one, which is approximately consistent with the enhancement ratio of 18.1% among the measured J_{SC} values. It should be pointed out that the calculated J_{SC} value slightly lower than the measured one in Table 1 is mainly ascribed to a smaller device area of 5 mm^2 than the light spot in the IPCE measurement, thereby leading to loss of a fraction of light in these devices. Because the IPCE depends on the light absorption in the active layer, the approximate enhancement factors from the measurement and calculation results indicate that the increased J_{SC} in the device with 20 nm ZnO/Au NRs/8 nm overlayer is due to the absorption improvement in the photoactive layer.

To further confirm our analysis above, we prepare two structures ITO/ZnO (28 nm)/P3HT: $PC_{60}BM$ and ITO/ZnO (20 nm)/Au NRs/ZnO (8 nm)/P3HT: $PC_{60}BM$ to measure their light absorption spectra as shown in Fig. 4. The inset shows an SEM image of Au NRs deposited on the ZnO layer surface, from which one observes that Au NRs are well dispersed on the bottom ZnO film with their longitudinal axes parallel to the film, but their orientations are arbitrary in the film. Besides, the Au NRs' density on the ZnO surface is calculated to be 120 particles/μm^2. The light absorption spectra in Fig. 4 show that Au NRs inserted between the two ZnO layers indeed improve the light absorption of P3HT:$PC_{60}BM$, consistent with our IPCE results. From the absorption spectrum of Au NRs in Fig. 1, we clearly find that the resonance peak excited by Au NR transverse axis is near maximum absorption wavelength of P3HT:$PC_{60}BM$, indicating that the enhanced light absorption in the active layer is attributed to the increased light field excited by Au NRs. As we know, when sunlight is incident on metallic NPs, the surface charges of metallic NPs interact with the electromagnetic field, then the electric field in the vicinity of metallic NPs is strongly increased due to the collective oscillations of surface electrons induced by incident light. The overlap between the LSPR wavelength and absorption band of active material will help to enhance the absorption efficiency of the solar cell. This is further proved to be true by calculating the incident electric field distribution within the devices (the effect of magnetic field is negligible, thus only electric field intensity is considered). From Figs. 5(a)–5(c), we can see that the electric field intensities are enhanced by inserting the Au NRs at 550, 600, and 635 nm, respectively. We also observe that among all the wavelengths, the electric field increase is the most obvious at 635 nm, which means that the LSPR wavelength moves towards a longer wavelength compared with the plasmonic peak of the transverse axis in aqueous solution in Fig. 1. We attribute this red shift to the fact that the refractive index of ZnO is higher than that of the aqueous solution.

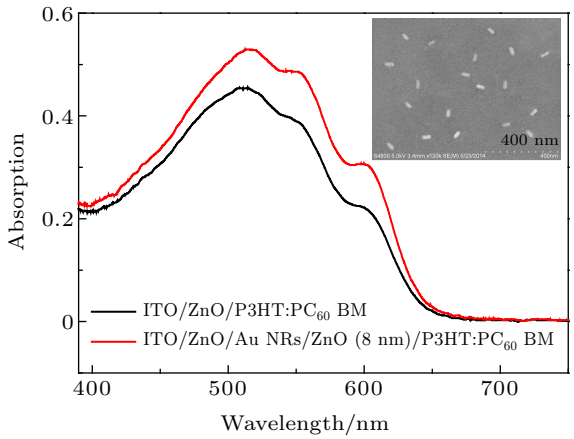


Fig. 4. (color online) Absorption spectra for the structures of ZnO (28 nm)/P3HT:$PC_{60}BM$ and ZnO (20 nm)/Au NRs/ZnO overlayer (8 nm) /P3HT:$PC_{60}BM$. The inset shows an SEM image of Au NRs spin-coated onto the ZnO film with a bar of 400 nm.

Note that the LSPR effect from the longitudinal axis is not effectively utilized because its plasmon resonance band fails to fall in the P3HT:$PC_{60}BM$ absorption range of 400–650 nm. It was reported that for the metallic NPs with small sizes of 5–20 nm, the near-field intensity generated by the LSPR effect is mainly responsible for the light harvesting enhancement. While for the larger size NPs, light scattering makes the incident light travel a longer path, thus giving rise to an obvious absorption increase within the active layer.[26–28] Figure 6 shows the simulation results of the light scattering cross sections of the glass/ITO/ZnO (28 nm) with/without Au NRs/P3HT:$PC_{60}BM$/MoO_3/Ag multilayer films. The scattering cross section (SCS) without Au NRs is about 10^{-28}, while it increases up to 10^{-18} when incorporating Au NRs into the ZnO extraction layer, about 10 orders of magnitude. From the above results, we speculate that light scattering from the longitudinal axis is beneficial to increasing light harvesting and

further raising the OPV's PCE because of the relatively large size Au NPs used in our experiments. The role of Au NRs' light scattering in absorption enhancement is also proved by comparing the plasmonic and its control devices in group 1. As shown in Table 1, the J_{SC} in the plasmonic device with a 20-nm ZnO overlayer increases from 7.91 to 8.47 mA/cm^2, corresponding to an enhancement factor of 7.1%. Figure 5(d) reveals that the variations of electric field intensity with the incident direction of sun light in the plasmonic devices with 8-nm and 20-nm ZnO overlayer and their control devices. It is clear that although the electric field increase induced by LSPR can be observed around Au NRs, the intensive local field can hardly reach the photoactive layer because of the thick ZnO overlayer between P3HT:PC$_{60}$BM and Au NRs, which means that Au NR-induced LSPR has no contribution to light harvesting enhancement in a thick ZnO overlayer, so we conclude that light scattering by Au NRs is the main factor for the J_{SC} improvement in the device with a 20-nm ZnO overlayer. While for an 8-nm ZnO overlayer, the electric field in the photoactive layer shows a significant enhancement. As shown in the inset in Fig. 5(d), the intensive local field induced by LSPR can extend to the depth of about 15 nm in P3HT:PC$_{60}$BM. Through our discussion above, we attribute the J_{SC} improvement in the plasmonic device with an 8-nm ZnO overlayer to the absorption enhancement in the photoactive layer induced by both Au NRs' LSPR effect and their scattering to the incident light.

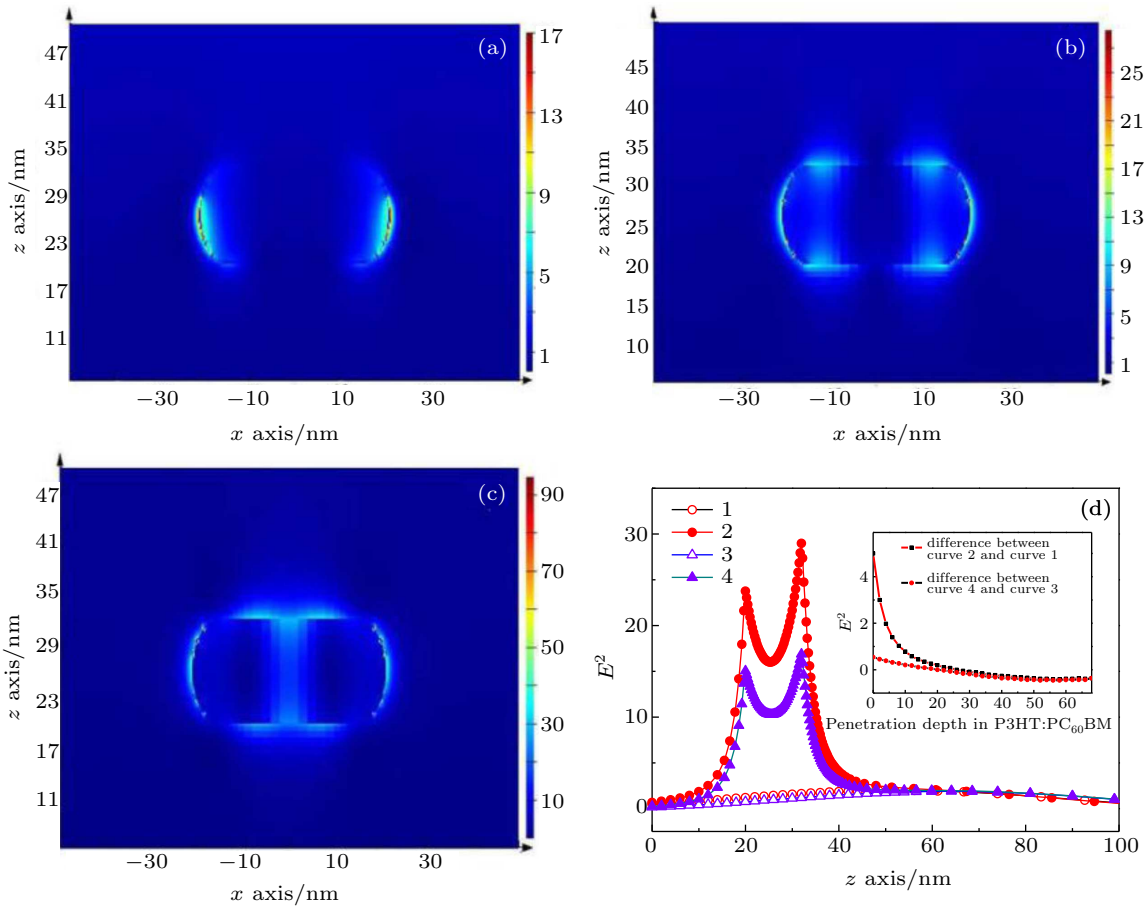


Fig. 5. (color online) Simulated electric field distributions around Au NR in the plasmonic device with 8-nm ZnO overlayer at (a) 550 nm, (b) 600 nm, and (c) 635 nm along the XZ plane. (d) Variances of the electric field intensity at 635 nm along the Z axis at $x = 0$ in the devices (1: ZnO (28 nm)/P3HT:PC$_{60}$BM; 2: ZnO (20 nm)/Au NRs/ ZnO (8 nm)/P3HT:PC$_{60}$BM; 3: ZnO (40 nm)/P3HT:PC$_{60}$BM; 4: ZnO (20 nm)/Au NRs/ZnO (20 nm)/P3HT:PC$_{60}$BM). The X and Z axes are along the longitudinal axis of Au NR and the incident direction of sun light, respectively. The inset shows the difference in electric field of P3HT:PC$_{60}$BM layer between the plasmonic and its control devices.

To investigate the influence of the insertion of Au NRs on the active layer morphology, we measure the morphologies of P3HT/PC$_{60}$BM with and without Au NRs by using atom force microscope (AFM). Figure 7 shows the typical height and phase images of P3HT/PC$_{60}$BM layer spin-coated on ZnO with and without Au NRs. We can see that the active layer with Au NRs is rougher than that without Au NRs, which has root-mean-squared surface roughness of 4.3 nm in Fig. 7(b) compared with 3.3 nm in Fig. 7(a). Besides, islands and valleys are apparent, while ordered P3HT chain alignment is clearly visible in Figs. 7(b) and 7(d), but they are absent in Figs. 7(a) and 7(c). These two features may be beneficial to the enhancement of charge transport in active layer and charge collection by electrode.

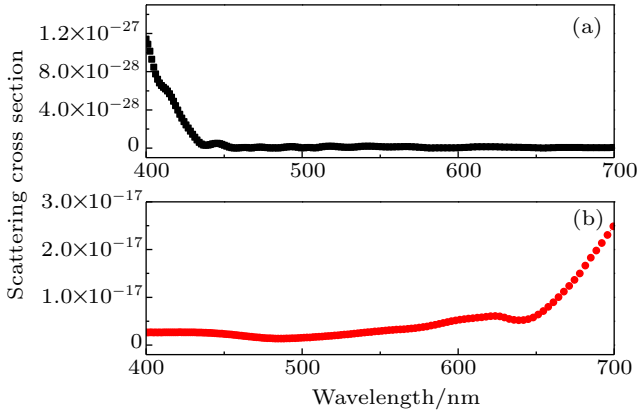


Fig. 6. (color online) Calculated scattering cross sections for glass/ITO/ZnO (28 nm) without (a) and with (b) Au NRs/P3HT:$PC_{60}BM$/MoO_3/Ag multilayer films.

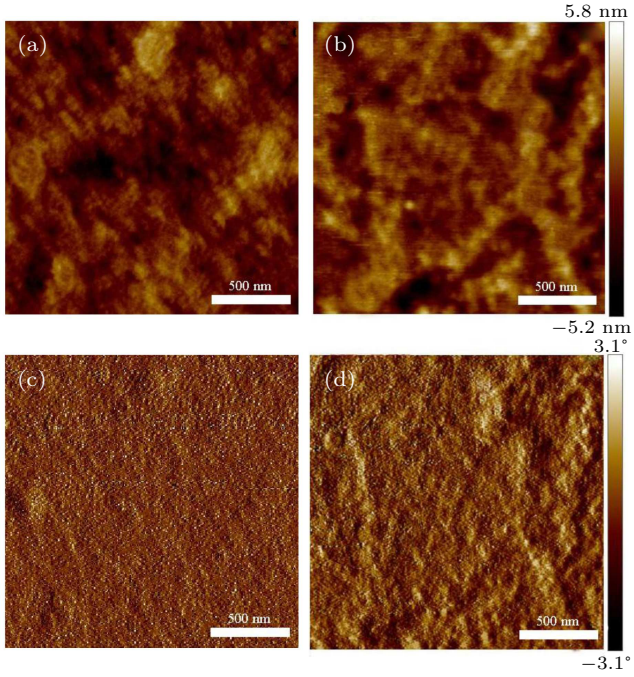


Fig. 7. (color online) AFM images of P3HT:$PC_{60}BM$ films spin-coated on ZnO without ((a), (c)) and with ((b), (d)) Au NRs. Panels (a) and (b) are height images, and panels (c) and (d) are phase images.

Unlike the improved performances in the device with a 20-nm or 8-nm ZnO overlayer, the device with an only 4-nm ZnO overlayer exhibits a seriously declined performance compared with its control device 3, which is mainly caused by low V_{OC} and FF values of 0.50 V and 0.45. Such a large V_{OC} and an FF loss indicate a direct contact of the Au NRs with P3HT:$PC_{60}BM$ due to a very thin ZnO overlayer, leading to a nonohmic contact between the electrode and the active layer.[29–31] To confirm our deduction, x-ray photoelectron spectroscopy (XPS) spectra of ZnO/Au NRs/ZnO (4 nm) and ZnO/Au NRs/ZnO (20 nm) are measured. Compared with that in the ZnO/Au NRs/ZnO (20 nm) multilayer in Fig. 8(a), the significant Au 4f signal intensity in the ZnO/Au NRs/ZnO (4 nm) multilayer in Fig. 8(b) confirms our speculation that the 4-nm ZnO cannot completely cover the Au NRs and the

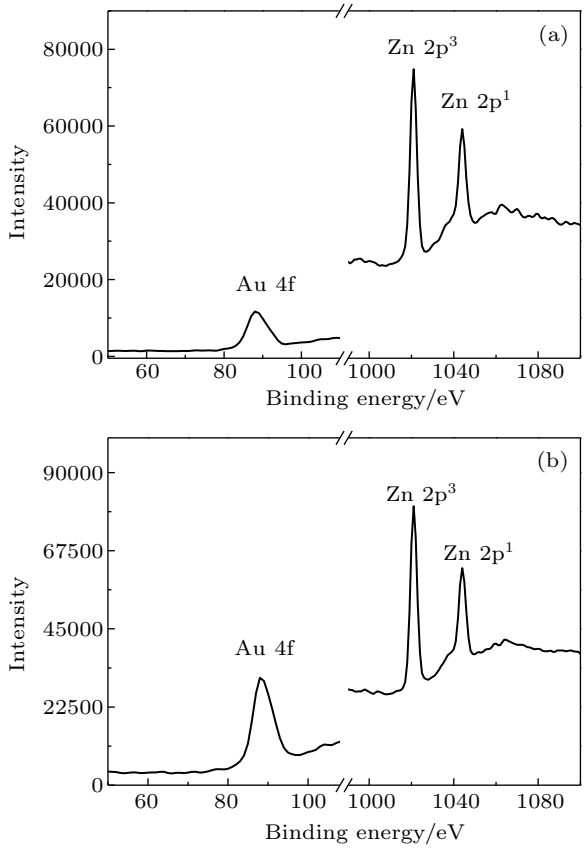


Fig. 8. XPS spectra of (a) ZnO/Au NRs/ZnO (20 nm) and (b) ZnO/Au NRs/ZnO (4 nm) multilayers.

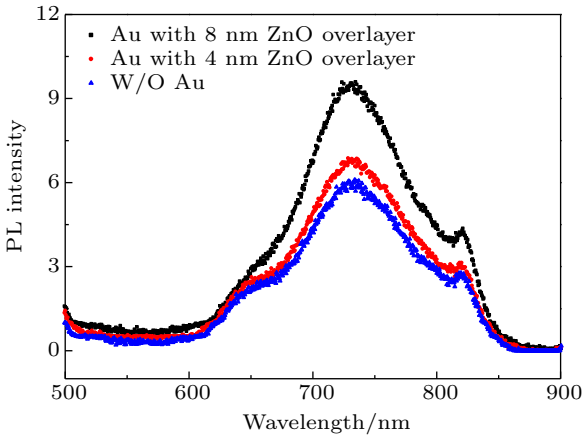


Fig. 9. (color online) PL spectra of three multilayers of ZnO/P3HT:$PC_{60}BM$, ZnO/Au NRs/ZnO (8 nm)/P3HT:$PC_{60}BM$, and ZnO/Au NRs/ZnO (4 nm)/P3HT:$PC_{60}BM$. A 480-nm laser is used as the excitation source.

exposure of most of the Au NRs under the P3HT:$PC_{60}BM$ active layer results in a non-ohmic contact between the cathode and the photoactive layer. Therefore, an increased interface energetic barrier due to a high work function of Au (5.1 eV) accounts for the decrease in V_{OC}.[31] Moreover, these exposed Au NRs serving as the recombination centers lead to the quenching of excitons in the vicinity of Au NRs, and thus a further decrease in FF. This can be proved with the measured photoluminescence (PL) spectra of three multilayers of ZnO/P3HT:$PC_{60}BM$, ZnO/Au NRs/ZnO (8 nm)/P3HT:$PC_{60}BM$, and ZnO/Au NRs/ZnO

(4 nm)/P3HT:$PC_{60}BM$ as shown in Fig. 9. By spin-coating an 8-nm ZnO layer on the top of Au NRs, the PL peak intensity of the photoactive layer is remarkably enhanced by 51% at 734 nm, meaning more photogenerated excitons due to the coupling between the plasmonic field of the Au NRs and the excited state of P3HT molecules. This is consistent with the improvement on the absorption and J_{SC}. In contrast, the obviously decreased PL intensity for the film with a 4-nm ZnO overlayer indicates that the excitons quenching in the vicinity of Au NRs is dominant when the inserted ZnO film between the Au NRs and the photoactive layer is too thin.

4. Conclusions

In this paper, we report the enhanced performance by sandwiching Au NRs between two layers of ZnO in the polymer solar cell with a structure of ITO/ZnO/Au NRs/ZnO overlayer/P3HT:$PC_{60}BM$/MoO_3/Ag. The J–V curves show that the device with an 8-nm ZnO overlayer exhibits the best performance with a PCE of 3.60% and a J_{SC} of 10.51 mA/cm^2, corresponding to increase of 19.6% and 18.1% compared with the control device. Our analysis reveals that the near-field strength induced by LSPR around Au NRs plays a major role in improving the absorption of P3HT:$PC_{60}BM$. In addition, light scattering from the longitudinal axis of Au NRs, resulting in the increase of OPL in active layer, may also be responsible for the absorption enhancement of active layer.

References

[1] Coakley K M and McGehee M D 2004 *Chem. Mater.* **16** 4533
[2] Moon J S, Takacs C, Cho S, Coffin R C, Kim H, Bazan G C and Heeger A J 2010 *Nano Lett.* **10** 4005
[3] Peet J M L, Senatore M L, Heeger A J and Bazan G C 2009 *Adv. Mater.* **21** 1521
[4] You J, Dou L, Yoshimura K, Kato T, Ohya K, Moriarty T, Emery K, Chen C, Gao J, Li G and Yang Y 2013 *Nat. Commun.* **4** 1446
[5] Zhou H, Zhang Y, Seier J, Collins S D, Luo C, Bazan G C, Nguyen T Q and Heeger A J 2013 *Adv. Mater.* **25** 1646
[6] Huang Q, Wang J, Cao L R, Sun J, Zhang X D, Geng W D, Xiong S Z and Zhao Y 2009 *Acta Phys. Sin.* **58** 1980 (in Chinese)
[7] Zhou R L, Chen X S, Zeng Y, Zhang J B, Chen H B, Wang S W, Lu W, Li H J, Xia H and Wang L L 2008 *Acta Phys. Sin.* **57** 3506 (in Chinese)
[8] Barnes W L, Dereux A and Ebbesen T W 2003 *Nature* **424** 824
[9] Xiang C P, Jin Y, Liu J T, Xu B Z, Wang W M, Wei X, Song G F and Xu Y 2014 *Chin. Phys. B* **23** 038803
[10] Mahmoud A Y, Zhang J, Ma D, Izquierdo R and Truong V V 2012 *Org. Electron.* **13** 3102
[11] Tan K S, Chuang M K, Chen F C and Hsu C S 2013 *ACS Appl. Mater. Interfaces* **5** 12419
[12] Hao J Y, Xu Y, Zhang Y P, Chen S F, Li X A, Wang L H and Huang W 2015 *Chin. Phys. B* **24** 045201
[13] Heo S W, Lee E J, Song K W, Lee J Y and Moon D K 2013 *Org. Electron.* **14** 1931
[14] Li X, Choy W C H, Lu H, Sha W E I and Ho A H P 2013 *Adv. Funct. Mater.* **23** 2728
[15] Wang D H, Kim D Y, Choi K W, Seo J H, Im S H, Park J H, Park O O and Heeger A J 2011 *Angew. Chem. Int. Ed.* **50** 5519
[16] Chen X, Zhao C, Rothberg L and Ng M K 2008 *Appl. Phys. Lett.* **93** 123302
[17] Heo M, Cho H, Jung J W, Jeong J R and Park S 2011 *Adv. Mater.* **23** 5689
[18] Morfa A J, Rowlena K L, Reilly T H, Romero M J and Lagemaatb J V D 2008 *Appl. Phys. Lett.* **92** 013504
[19] Qu D, Liu F, Huang Y, Xie W and Xu Q 2011 *Opt. Express* **19** 24795
[20] Wu B, Wu X, Guan C, Tai K F, Yeow E K L, Fan H J, Mathews N and Sum T C 2013 *Nat. Commun.* **4** 2004
[21] Anger P, Bharadwaj P and Novotny L 2006 *Phys. Rev. Lett.* **96** 113002
[22] Chen S F, Cheng F, Mei Y, Peng B, Kong M, Hao J Y, Zhang R, Xiong Q H, Wang L H and Huang W 2014 *Appl. Phys. Lett.* **104** 213903
[23] Zhou J, Xue M, Shen H, Wu Z, Kim S and Ho J J 2011 *Appl. Phys. Lett.* **98** 151110
[24] Janković V, Yang Y, You J, Dou L, Liu Y, Cheung P, Chang J P and Yang Y 2013 *ACS Nano* **7** 3815
[25] Lu L, Luo Z, Xu T and Yu L 2013 *Nano Lett.* **13** 59
[26] Atwater H A and Polman A 2010 *Nat. Mater.* **9** 205
[27] Dijk M A V, Tchebotareva A L, Orrit M, Lippitz M, Berciaud S, Lasne D, Cognetc L and Lounisc B 2006 *Phys. Chem. Chem. Phys.* **8** 3486
[28] Hsiao Y S, Charan S, Wu F Y, Chien F C, Chu C W, Chen P and Chen F C 2012 *J. Phys. Chem. C* **116** 20731
[29] Kim K and Carroll D L 2005 *Appl. Phys. Lett.* **87** 203113
[30] Mihailetchi V D, Blom P W M, Hummelen J C, Rispens M T 2003 *J. Appl. Phys.* **94** 6849
[31] Sun J, Zhu Y, Xu X, Lan L, Zhang L, Cai P, Chen J, Peng J and Cao Y 2012 *J. Phys. Chem. C* **116** 14188